

## Solvation effects on the molecular 3s Rydberg state: AZAB/CYCLO octanes clustered with argon

Q. Y. Shang, P. O. Moreno, S. Li, and E. R. Bernstein

Citation: *The Journal of Chemical Physics* **98**, 1876 (1993); doi: 10.1063/1.464222

View online: <http://dx.doi.org/10.1063/1.464222>

View Table of Contents: <http://aip.scitation.org/toc/jcp/98/3>

Published by the *American Institute of Physics*

---

---

**COMPLETELY**

**REDESIGNED!**



**PHYSICS  
TODAY**

*Physics Today* Buyer's Guide  
Search with a purpose.

# Solvation effects on the molecular 3s Rydberg state: AZAB/CYCLO octanes clustered with argon

Q. Y. Shang, P. O. Moreno, S. Li, and E. R. Bernstein  
Colorado State University, Chemistry Department, Fort Collins, Colorado 80523

(Received 13 July 1992; accepted 15 October 1992)

Two color, 1 + 1, mass resolved excitation spectroscopy (MRES) is used to obtain molecular Rydberg ( $3s \leftarrow n$ ) spectra of azabicyclo[2.2.2]octane (ABCO) and diazabicyclo[2.2.2]octane (DABCO) clustered with argon. Nozzle/laser timing delay studies are employed together with time-of-flight mass spectroscopy to identify cluster composition. Population depletion techniques are used to differentiate between clusters with the same mass, but different geometries. A Lennard-Jones 6–12 potential is used to model the intermolecular interactions and predict minimum energy cluster geometries and cluster binding energies. The experimental results are combined with the cluster geometry calculations to assign spectral features to specific cluster geometries. Three different excited state interactions are required to model the experimentally observed line shapes, spectral shifts, and cluster dissociation. The relationship between these model potentials and the cluster binding sites suggests that the form of the cluster intermolecular potential in the Rydberg excited state is dictated by the distance between the argon and chromophore atoms. A comparison of results for  $\text{ABCO}(\text{Ar})_1$  and  $\text{DABCO}(\text{Ar})_1$  leads to the conclusion that the nitrogen 3s Rydberg orbital in clusters of DABCO is delocalized.

## I. INTRODUCTION

Rydberg spectroscopy is generally thought to involve the promotion of an electron from a nonbonded, lone-pair,  $\sigma$ -bond, or  $\pi$ -bond orbital to a nonbonding orbital of higher principal quantum number. These extravalent orbitals are currently viewed as being localized, atomic like, nonbonding orbitals which have a large spatial distribution and are therefore very polarizable.<sup>1</sup> The extended spatial distribution of these Rydberg orbitals is currently thought to make them extremely sensitive to external perturbations. In fact, their sensitivity to a high bath gas pressure has been embraced by experimentalists as the primary tool for distinguishing Rydberg transitions from valence transitions.<sup>1</sup> Until recently, the investigation of the characteristics of molecular Rydberg states has been neglected compared to those of valence states. This has been largely due to the difficulty of accessing Rydberg transitions, most of which are in the vacuum ultraviolet; however, a number of present technologies facilitate the study of molecular Rydberg transitions. The most consequential is the tunable dye laser which makes multiphoton spectroscopy a viable and valuable technique.<sup>2</sup> Multiphoton excitations may be used to access high energy transitions with two photon resonances so that the laser wavelength can be in the 500 to 200 nm range. This technique has the added advantage of probing transitions which are forbidden by a one photon absorption. Additionally, multiphoton ionization (MPI) provides for highly sensitive mass resolved detection. When used in conjunction with molecular jet techniques, mass resolved MPI provides a powerful means of studying cold molecular clusters. These studies provide direct quantitative information about external solvent perturbations.

The first study of Rydberg transitions in jet-cooled clusters has been recently performed on the cyclic ether

1,4-dioxane clustered with a number of nonpolar solvents.<sup>3</sup> Three binding sites in the ground state are determined. In all cases, the transition to the Rydberg state weakens the intermolecular interaction with the solvent, as is evidenced by the large blue shift of the transition energy. Such an effect differs significantly for different binding sites. This is the first study which shows, on a molecular level, effects of the Rydberg transition on the intermolecular interaction. Nonetheless, this study is deficient in that the observed Rydberg spectra cannot be correlated with specific cluster geometries. Therefore, the extent of the spatial distribution of the Rydberg orbital cannot be probed for this system.

Systems which are particularly amenable to these types of studies are the two caged tertiary amines, diazabicyclo[2.2.2]octane (DABCO) and azabicyclo[2.2.2]octane (ABCO). The transition of a nitrogen lone pair electron to the nitrogen 3s orbital ( $3s \leftarrow n$ ) in these molecules occurs at less than  $40\,000\text{ cm}^{-1}$ , allowing access by one photon of uv or two photons of visible laser light. DABCO has  $D_{3h}$  symmetry and the 3s state was originally studied by Parker and Avouris by both one and two photon excitation.<sup>4</sup> They concluded from their laser polarization studies that the 3s Rydberg state is totally symmetric, one photon forbidden, and two photon allowed. ABCO has  $C_{3v}$  symmetry which makes its  $3s \leftarrow n$  transition both one and two photon allowed. The one and two photon MPI spectra of supersonic jet-cooled ABCO and DABCO have also been acquired;<sup>5</sup> however, these studies are not mass resolved. Other efforts have probed the theoretical<sup>6</sup> and experimental<sup>7</sup> aspects of the relative importance of through-space and through-bond interactions of the nitrogen lone pair orbitals in the ground electronic state of DABCO. The latter studies have found that these nitrogen–nitrogen lone pair interactions have a pro-

found effect on electron distribution amongst ground state molecular orbitals.

In the following discussion, we report the  $3s \leftarrow n$  Rydberg spectra acquired by multiphoton ionization spectroscopy of DABCO and ABCO clustered with as many as four argon atoms. Cluster composition is identified with time-of-flight mass spectroscopy in combination with nozzle/laser timing delay studies. Population depletion techniques are employed to differentiate features which arise from different cluster geometries. The interpretation of these results is further supported by simple model calculations. Clustering of ABCO and DABCO with this simple solvent directly probes the effects of external perturbation on their  $3s \leftarrow n$  transition. Also, due to the high symmetry of these molecules, the shift of the origin transition can be directly correlated with solvent binding site, yielding information about the spatial extension of the Rydberg  $3s$  orbital. Furthermore, since lone pair interaction is not possible in the case of ABCO, a comparison of the  $\text{DABCO}(\text{Ar})_1$  and  $\text{ABCO}(\text{Ar})_1$  cluster spectra yields information about the extent of Rydberg orbital delocalization in DABCO.

## II. PROCEDURES

### A. Experiment

Mass resolved excitation spectra (MRES) of ABCO, DABCO, and their clusters with argon are acquired by employing a pulsed supersonic molecular jet expansion in combination with two color 1+1 or 2+1 multiphoton ionization (MPI). A detailed description of the supersonic molecular jet apparatus and time-of-flight mass spectrometer has been published previously.<sup>8</sup> For two color multiphoton ionization, two Nd/YAG pumped dye lasers (Spectra Physics) are employed. The dye laser fundamental of R590 (Exciton), R575 (Exciton), or F548 (Exciton) in methanol (ca. 10 mj/pulse) is used without focusing for the two photon excitation of DABCO (Aldrich, 98%). For the one photon excitation of DABCO, these dye fundamental frequencies are doubled with a KDP nonlinear crystal. The dye laser fundamental of a 1.3:1 mixture of LDS698/DCM (Exciton) in methanol is doubled and then mixed with the Nd/YAG 1.064  $\mu\text{m}$  fundamental to produce a uv beam for the one photon excitation of ABCO (Aldrich, 97%). The fundamental of C460 (Exciton) is used to ionize the excited species for all one and two photon excitations. Following ionization, the molecular and cluster ions are separated and analyzed by time-of-flight mass spectroscopy. Nozzle backing pressure is maintained at 50 psig. The solute, ABCO or DABCO, is used without additional purification and is placed in the head of the molecular jet nozzle which is heated to ca. 50  $^\circ\text{C}$  to vaporize the solid sample. For cluster studies, the bath gas (helium) is seeded with 0.1%–10% of argon (General Air, Commercial Grade).

Population depletion studies have been fully described previously.<sup>9</sup> The following details are specific to these experiments. Two Nd/YAG pumped dye lasers are used, one for population depletion and one for MPI detection

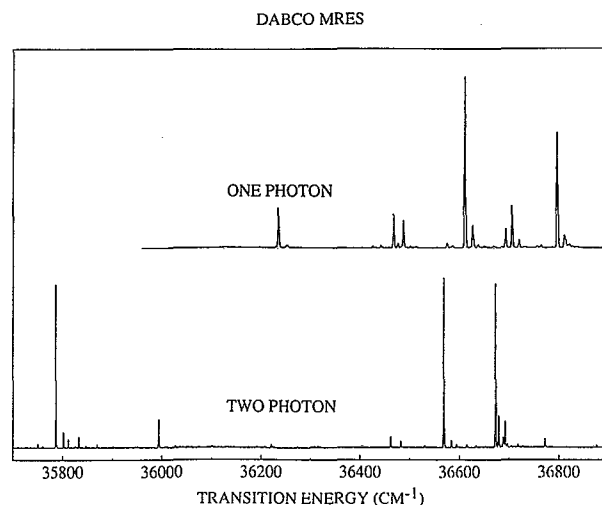


FIG. 1. Two photon (2+1) (bottom trace) and one photon (1+1) (top trace) two color mass resolved excitation spectrum (MRES) of DABCO. The electronic origin ( $0_0^0$ ) at 35 786.3  $\text{cm}^{-1}$  is two photon allowed and one photon forbidden.

(probe). The depletion and the probe lasers both employ the frequency doubled fundamental of R575 (Exciton). The resulting laser beams are each focused with a 1 m lens.

The ionization threshold for ABCO, DABCO, and their argon clusters is quite sharp (10%–90% ca. 20–50  $\text{cm}^{-1}$ ). All two color ionization data reported are obtained within 100  $\text{cm}^{-1}$  of the appropriate ionization threshold value for the system interrogated. For example, the ioniza-

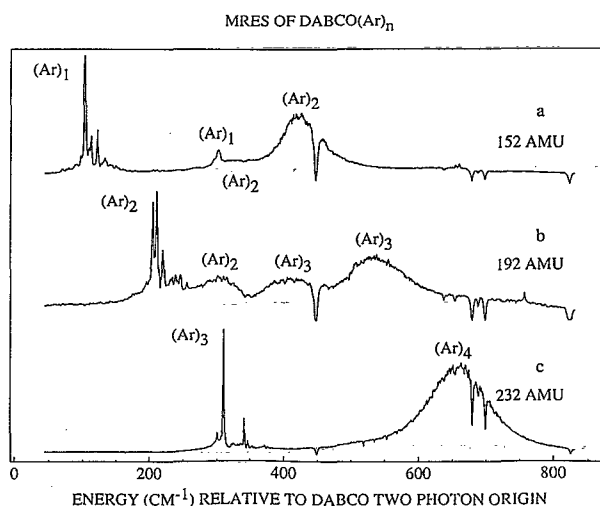


FIG. 2. One photon two color (1+1) MRES of  $\text{DABCO}(\text{Ar})_{1,2,3}$  clusters. The x-axis labels represent transition energies relative to the DABCO bare molecule two photon origin ( $0_0^0$ ) at 35 786.3  $\text{cm}^{-1}$ . Traces a (top), b (middle), and c (bottom) are acquired in mass channels 152, 192, and 232 amu, respectively. Individual features in the three traces are identified as specific  $\text{DABCO}(\text{Ar})_n$  cluster sizes with the use of laser/nozzle delay studies. Labels which identify the cluster size of each feature are abbreviated, i.e.,  $\text{DABCO}(\text{Ar})_1$  is written  $(\text{Ar})_1$ , and  $\text{DABCO}(\text{Ar})_2$  as  $(\text{Ar})_2$ , etc.

tion energy for the  $0_0^0$  transition of DABCO is  $22\,140\text{ cm}^{-1}$  above the transition energy. The threshold is at  $\sim 57\,930\text{ cm}^{-1}$ . For  $\text{DABCO}(\text{Ar})_1$  ( $0_0^0$  at  $35\,890.2\text{ cm}^{-1}$ ) the ionization photon energy is  $21\,920\text{ cm}^{-1}$ .

Nozzle/laser timing delay studies exploit the differences in velocity and formation time of clusters of different mass (size) after they are formed in the supersonic expansion. This arrival time difference may be detected by varying the delay between the nozzle pulse and the laser pulse. The distance between the nozzle and the ionization point is  $7.0\text{ cm}^{-1}$  in these experiments. These experiments have also been described previously.<sup>10</sup>

## B. Calculation

The ground state minimum energy cluster geometries for the  $\text{DABCO}(\text{Ar})_n$  ( $n=1,2,3$ ) and  $\text{ABCO}(\text{Ar})_1$  clusters are calculated using a Lennard-Jones 6–12 potential to model the atom–molecule van der Waals (vdW) interaction. The potential parameters and methods of Scheraga are used with fixed solvent and solute geometries, while their relative positions are energy optimized.<sup>11</sup> These calculations employ as many as 2000 randomly generated starting points. Normal mode analyses performed on these calculated cluster geometries have been described in detail elsewhere.<sup>12</sup>

## III. RESULTS

### A. $\text{DABCO}(\text{Ar})_n$

#### 1. Experiment

Figure 1 displays the one and two photon MRES of the bare jet-cooled DABCO molecule in the region of its two photon allowed  $3s \leftarrow n$  origin ( $0_0^0$ ) at  $35\,786\text{ cm}^{-1}$ . The bottom trace represents the two photon transitions, while the top trace represents the one photon transitions. The one and two photon transition energies are listed in Table I. These spectra are in agreement with previously reported jet cooled MPI spectra which are not mass resolved.<sup>5</sup>

Seeding the molecular beam with 1% of argon results in the observation of one photon MRES of  $\text{DABCO}(\text{Ar})_n$ , where  $n=1,2,3,4,5$ . Two photon spectra of these clusters are not observed, most likely due to the small cross section for the process and the reduced cluster concentration. The two color, one photon MRES of the  $n=1, 2$  and 3 mass channels are represented by the top (a), middle (b), and bottom (c) traces in Fig. 2, respectively. In this plot, the  $x$ -axis labels represent the one photon transition energies relative to the DABCO bare molecule  $0_0^0$  transition at  $35\,786\text{ cm}^{-1}$ . One photon absorption to the  $0^0$  level of  $\text{DABCO}(\text{Ar})_n$  is observed due to the reduced symmetry of the clusters with respect to the bare molecule (see below). The negative peaks are due to detector saturation from the

TABLE I. Transition energies and assignments for DABCO, ABCO, and their clusters with argon.

Cluster (Mass)	Description	Transition energies ( $\text{cm}^{-1}$ )	Relative energies ( $\text{cm}^{-1}$ )		Assignment <sup>a</sup>
			Origin	Vibrations	
DABCO		35 786.3	0.0		0–0
2 photon		36 568.0		781.7	$\nu_3'$
		36 673.0		886.7	$\nu_2'$
		36 692.2		905.9	$\nu_\alpha'$
		36 236.6		450.3	$\nu_{27}'(e')$
DABCO	1 photon	36 611.8		825.5	$\nu_{26}'(e')$
		36 706.5		920.2	$\nu_\omega'$
		36 797.9		1011.6	$\nu_{20}'(e')$
$\text{DABCO}(\text{Ar})_1$	(152.1 amu)	sharp	35 890.2	103.9	0–0
	(152.1 amu)	sharp	35 899.4		vdW
	(152.1 amu)	sharp	35 908.5		vdW
	(152.1 amu)	broad	36 076.0	290.0	0–0
$\text{DABCO}(\text{Ar})_2$	(192.1 amu)	sharp	35 992.4	206.1	0–0
	(192.1 amu)	sharp	35 998.0		vdW
	(192.1 amu)	sharp	36 007.4		vdW
	(192.1 amu)	broad	36 066.0	280.0	0–0
	(152.1 amu)	broad	36 161.0	375.0	0–0
$\text{DABCO}(\text{Ar})_3$	(232.0 amu)	sharp	36 086.3	300.0	hot band
	(232.0 amu)	sharp	36 096.3	310.0	0–0
	(192.1 amu)	broad	36 156.0	380.0	0–0
	(192.1 amu)	broad	36 276.0	490.0	0–0
ABCO		39 101.6	0.0		0–0
		39 234.3		132.7	$\nu_x'$
$\text{ABCO}(\text{Ar})_1$	(151.1 amu)	sharp	39 074.0	–27.6	0–0
	(151.1 amu)	sharp	39 149.0	47.0	0–0
	(151.1 amu)	broad	39 347.0	245.0	0–0

<sup>a</sup>vdW denotes intermolecular van der Waals modes and  $\nu_x'$  implies molecular vibrations in the excited state.

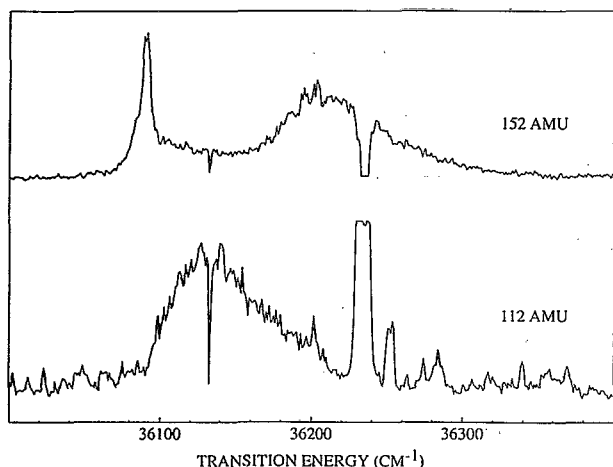


FIG. 3. One photon excitation, two color (1+1) MRES illustrates the DABCO(Ar)<sub>1</sub> cluster (mass=152 amu) dissociating into the DABCO bare molecule (mass=112 amu) mass channel. The cluster giving rise to the broad feature in the 152 amu mass channel dissociates at about 36 100 cm<sup>-1</sup> and its signal simultaneously appears in the 112 amu mass channel.

bare DABCO molecule signal which is approximately 15 times more intense than the  $n=1$  cluster signal. Both the sharp and broad features in these spectra are to the blue of the bare molecule  $0_0^0$ . These cluster spectra do not display any features to the red of the bare molecule two photon  $0_0^0$ . The transition energies of the sharp features and the low energy edge of the broad features are listed in Table I. Signal is also observed in the DABCO(Ar)<sub>4,5</sub> mass channels. The spectra in these mass channels are broad, devoid of sharp features, and the apparent origin is blue shifted further than the DABCO(Ar)<sub>1,2,3</sub> spectral features.

In the spectrum appearing in the 152 amu mass channel [trace (a) of Fig. 2], the first broad feature begins 300 cm<sup>-1</sup> to the blue of the DABCO  $0_0^0$  and then exhibits a sharp dropoff after approximately 20 cm<sup>-1</sup>. The top trace in Fig. 3 is an expanded view of this region of the 152 amu mass channel spectrum. The bottom trace in Fig. 3 shows that coincident with the disappearance of signal in the 152 amu mass channel at 307 cm<sup>-1</sup> is the appearance of signal in the 112 amu mass channel. This latter signal is not observed when argon is absent from the molecular beam. The observation of van der Waals (vdW) cluster signal appearing in a lower mass channel is typical of cluster dissociation.

Nozzle/laser timing delay studies are performed to determine whether dissociation is occurring in the higher order clusters and contributing to spectra being detected in lower mass channels. Figure 4 shows intensity profiles of signal arising from different sized clusters as a function of nozzle/laser timing delay. These profiles show the differences in nozzle-to-laser flight times for clusters of differing mass. There is a minor contribution to these flight times from the specific cluster formation dynamics, and a major contribution from the cluster velocity which depends on the cluster mass. The results of these experiments are indicated in Fig. 2 by the abbreviated labels on each spectral

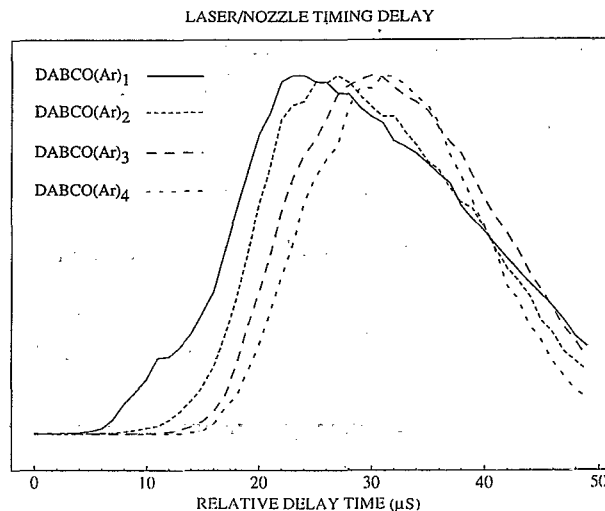


FIG. 4. One photon, two color (1+1) MRES signal intensity versus nozzle/laser delay time ( $\mu$ s). Delay times are relative.

feature. These timing delay studies are calibrated with the sharp features in each mass channel which show no signs of dissociation.

The most intense sharp feature in trace (a) of Fig. 2 is shifted 103.9 cm<sup>-1</sup> to the blue of the bare molecule origin. This feature is identified with the DABCO(Ar)<sub>1</sub> cluster mass from the nozzle/laser timing delay study. The second feature in this spectrum starts to gain intensity at about 290 cm<sup>-1</sup> to the blue of the bare molecule origin and is also identified with the DABCO(Ar)<sub>1</sub> cluster. Mentioned above, and demonstrated in Fig. 3, the sharp decrease in signal at the blue edge of this feature coincides with the appearance of a broad feature in the bare molecule mass channel (112 amu). This broad feature persists in the 152 amu mass channel for  $\sim 20$  cm<sup>-1</sup> and then vanishes due to dissociation of the cluster and persists in the 112 amu mass channel for another  $\sim 100$  cm<sup>-1</sup>. A broad signal, underlying and just to the blue of this feature in the 152 amu mass channel, is identified with DABCO(Ar)<sub>2</sub>. This is coincident with a decrease of signal in the 192 amu mass channel and can be attributed to the dissociation of DABCO(Ar)<sub>2</sub> into the 152 amu mass channel. Similarly, the third prominent feature in trace a of Fig. 2, beginning at approximately 380 cm<sup>-1</sup> to the blue of the bare molecule origin, is identified by the nozzle/laser timing delay study as originating from the DABCO(Ar)<sub>2</sub> cluster and is labeled accordingly.

Population depletion techniques can differentiate between clusters of the same mass, but with different geometries. This approach is a cross between a hole burning and an ion dip experiment. In a population depletion experiment, the molecular beam of mixed species is excited with an intense laser (depletion laser) and the MRES of the resulting beam is then probed at a different frequency with another laser (probe laser) of reduced intensity. The probe laser is fixed at a cluster resonance peak. The depletion laser scans the spectral region and depletes the ground

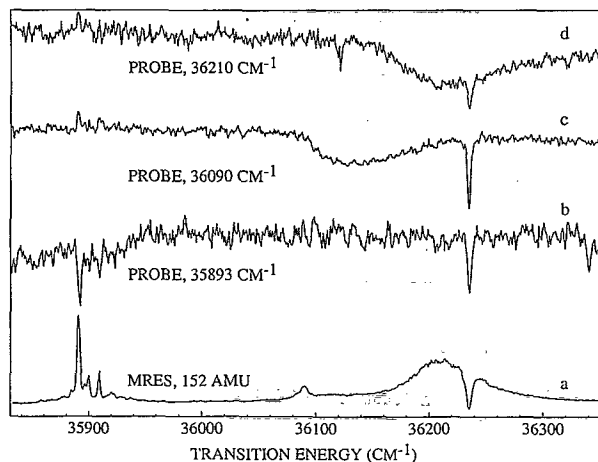


FIG. 5. Population depletion spectra acquired at a mass of 152 amu (traces b, c, d) and the one photon, two color (1+1), MRES acquired in this mass channel (trace a). Labels indicate the probe laser energy for the population depletion spectra (top three traces). The dip in signal at 36 236  $\text{cm}^{-1}$  in all four traces is due to detector saturation from a bare molecule vibronic feature.

state population of any cluster species for which it is in resonance. The result is that the signal associated with the probe laser will be decreased when the depletion laser scans through a resonance of the cluster species being probed. This experiment yields three important determinations. First, it can distinguish whether two features which are observed in the same mass channel result from the same, or from different cluster geometries. Second, it can verify the results of the nozzle/laser timing delay study. Third, population depletion studies support the determination that cluster dissociation occurs in the  $S_1$  state of the neutral cluster and not the cluster ion because the full spectrum of dissociating clusters is observed in this experiment.

The results of such a study for  $\text{DABCO}(\text{Ar})_1$  are shown in Fig. 5. The x-axis labels are the population depletion energies in wave numbers. The negative peak which appears at 36 236  $\text{cm}^{-1}$  in all four traces is due to detector saturation from a bare molecule vibronic transition. Trace (a) of Fig. 5 is the MRES acquired in the 152 amu mass channel and is identical to trace (a) of Fig. 2. The next trace, (b), is acquired with a probe laser energy of 35 893  $\text{cm}^{-1}$  which corresponds to the transition energy of the most intense sharp feature in trace (a) of Fig. 5. In trace (b) of Fig. 5, the depletion laser only affects the probe signal at the probe laser energy (a trivial result) and at the transition energies of the two less intense sharp features just to the blue of this. Therefore, the small sharp features to the blue of 35 893  $\text{cm}^{-1}$  arise from the same cluster species as it does, and the two features centered at 36 090  $\text{cm}^{-1}$  and 36 210  $\text{cm}^{-1}$  do not.

An equivalent analysis is applied to trace (c) of Fig. 5. In this spectrum the probe laser energy is 36 090  $\text{cm}^{-1}$  and the probe signal is affected by the depletion laser only at energies corresponding to some broad feature beginning at 36 080  $\text{cm}^{-1}$ . Therefore, this broad feature arises from a different cluster species than both the sharp feature at

35 893  $\text{cm}^{-1}$  and the broad feature centered at 36 210  $\text{cm}^{-1}$ . Notice that the dissociation of the cluster upon excitation at 36 100  $\text{cm}^{-1}$  does not prohibit the detection of population depletion for the rest of this broad feature from 36 100 to 36 200  $\text{cm}^{-1}$ . This confirms that the signal from 36 100 to 36 200  $\text{cm}^{-1}$  in the bottom trace of Fig. 3 is a result of the same cluster species which gives rise to the signal from 36 080 to 36 100  $\text{cm}^{-1}$  in the top trace of Fig. 3.

Trace (d) of Fig. 5 shows the effect of the population depletion laser when the probe laser energy is 36 210  $\text{cm}^{-1}$ . The reduction of probe signal from 36 160 to 36 300  $\text{cm}^{-1}$  confirms what is shown above; this signal originates from a different cluster species that gives rise to the features at 35 893 and 36 090  $\text{cm}^{-1}$ . Population depletion experiments on the higher order clusters cannot be performed due to insufficient signal.

The results of the nozzle/laser timing delay and population depletion experiments allow us to return to Fig. 2 and make cluster size assignments for each sharp and broad feature observed in the MRES of traces (b) and (c). The sharp features which appear in trace (b) of Fig. 2, 206.1  $\text{cm}^{-1}$  to the blue of the bare molecule origin, are determined by the nozzle/laser timing delay study to be due to the  $\text{DABCO}(\text{Ar})_2$  cluster. The next feature in this trace is broad, beginning about 280  $\text{cm}^{-1}$  to the blue of the bare molecule  $0_0^0$  transition, and continues to gain intensity for about 40  $\text{cm}^{-1}$ . This feature then begins to lose intensity in the 192 amu mass channel and appears in the 152 amu mass channel. This feature is due to the  $\text{DABCO}(\text{Ar})_2$  cluster. The next broad feature in trace (b) of Fig. 2 begins to appear at about 370  $\text{cm}^{-1}$  to the blue of the bare molecule origin, is centered at 410  $\text{cm}^{-1}$ , and is determined to be due to the  $\text{DABCO}(\text{Ar})_3$  cluster. The last broad feature in this spectrum begins at about 490  $\text{cm}^{-1}$  to the blue of the bare molecule origin, is centered at 530  $\text{cm}^{-1}$ , and is also associated with  $\text{DABCO}(\text{Ar})_3$ .

Trace (c) of Fig. 2 has two main features. The most intense sharp feature is 310.0  $\text{cm}^{-1}$  to the blue of the bare molecule origin and is determined to be due to  $\text{DABCO}(\text{Ar})_3$ . The intense broad feature is centered at 660  $\text{cm}^{-1}$  and is determined to be due to  $\text{DABCO}(\text{Ar})_4$  dissociation.

## 2. Calculation

Minimum energy cluster geometry calculations for the  $\text{DABCO}(\text{Ar})_n$  clusters are performed employing a Lennard-Jones 6-12 empirical potential function. These calculations produce three cluster geometries for the  $\text{DABCO}(\text{Ar})_1$  cluster. A normal mode analysis is performed on these three cluster geometries to determine the magnitude of their vdW modes. These three cluster geometries are shown in Fig. 6(a) along with their respective binding energies (BE). In the most stable cluster geometry ( $\text{BE}=232 \text{ cm}^{-1}$ ) the argon atom lies in the  $\sigma_h$  plane midway between the two nitrogen atoms and directly above the center of a rectangle defined by four carbon atoms of one ring. This cluster geometry has three vdW mode frequencies which are 34.1  $\text{cm}^{-1}$  for the  $\text{DABCO}-\text{Ar}$  stretch, 28.8

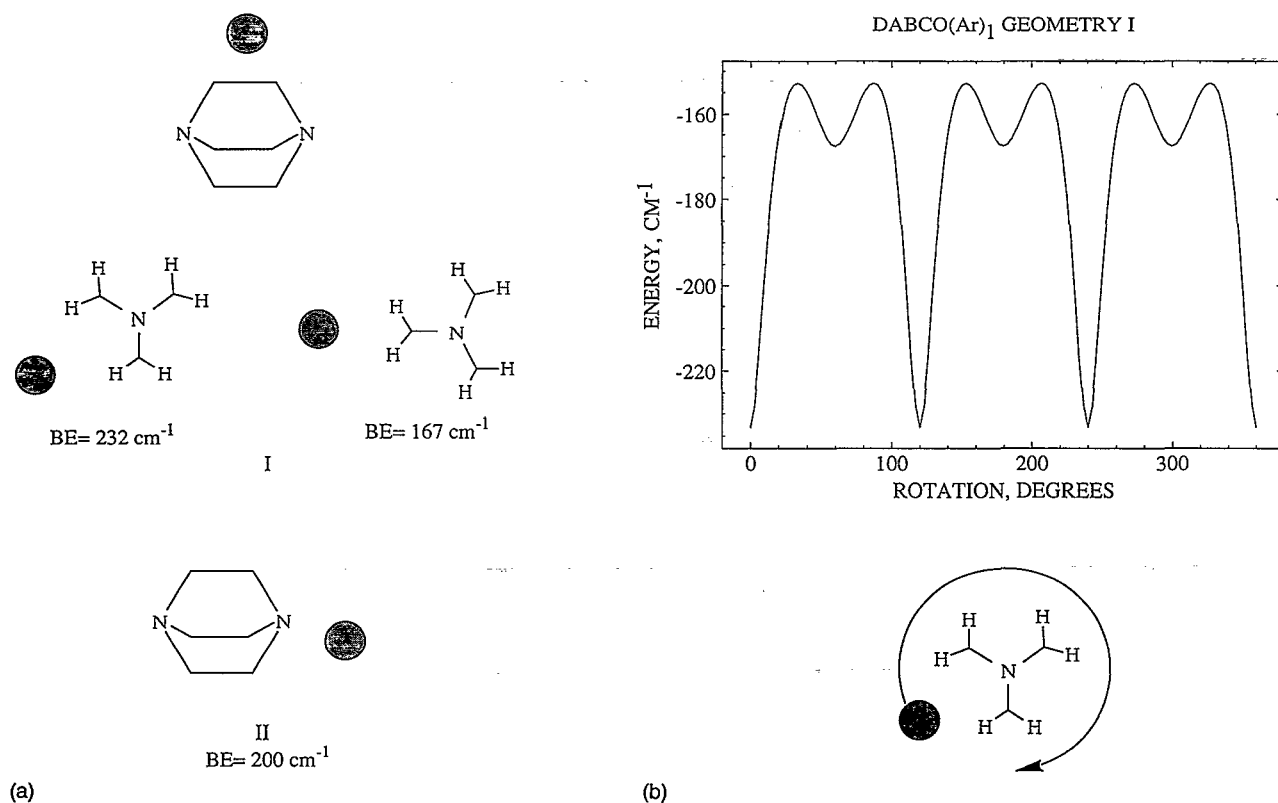


FIG. 6. (a) Minimum energy geometries of the  $\text{DABCO}(\text{Ar})_1$  cluster, simulated with a Lennard-Jones potential, and their binding energies (BE). The top picture shows the two calculated geometries in which the argon atom is in the  $\text{DABCO } \sigma_h$  plane. The bottom picture shows the calculated geometry in which the argon atom is near the  $\text{DABCO}$  nitrogen, along its  $C_3$  axis. (b) The top picture illustrates the movement of the argon atom around the  $\text{DABCO}$  molecule in the  $\sigma_h$  plane while minimizing the  $\text{DABCO-Ar}$  potential energy. The resulting potential energy profile is shown by the graph in the bottom picture. The  $x$ -axis labels represent the degree of rotation about the  $\text{DABCO}$  molecule in degrees and the  $y$ -axis labels represent the cluster atom-molecule potential energy in  $\text{cm}^{-1}$ . The  $14 \text{ cm}^{-1}$  barrier between the conformers is not large enough to confine the least stable calculated geometry ( $\text{BE} = 167 \text{ cm}^{-1}$ ) even at low temperature.

$\text{cm}^{-1}$  for the bend in which the argon moves in the  $\sigma_h$  plane, and  $26.0 \text{ cm}^{-1}$  for the bend in which the argon moves toward the  $\text{DABCO}$  nitrogens. The least stable geometry ( $\text{BE} = 167 \text{ cm}^{-1}$ ) also has the argon atom midway between the two nitrogen atoms, but lying next to a C-C bond, in a plane containing the two nitrogen atoms and the C-C bond. This cluster geometry has three vdW mode frequencies which are  $29.7 \text{ cm}^{-1}$  for the  $\text{DABCO-Ar}$  stretch,  $16.6 \text{ cm}^{-1}$  for the bend in which the argon moves in the  $\sigma_h$  plane,  $8.6 \text{ cm}^{-1}$  for the bend in which the argon moves toward the  $\text{DABCO}$  nitrogens. The third cluster geometry ( $\text{BE} = 200 \text{ cm}^{-1}$ ) the argon atom lies at the end of the molecule, near one of the nitrogen atoms, slightly off the  $C_3$  axis, and midway between two C-N-C carbon atoms. This cluster geometry has three vdW mode frequencies which are  $32.7 \text{ cm}^{-1}$  for the  $\text{DABCO-Ar}$  stretch,  $15.5 \text{ cm}^{-1}$  for one bend, and  $12.7 \text{ cm}^{-1}$  for the other bend.

To determine the potential barrier between the most stable and least stable cluster geometries, a potential energy profile is calculated by moving the argon atom around the  $\text{DABCO}$  molecule in the  $\sigma_h$  plane while optimizing the  $\text{DABCO-Ar}$  distance. This potential energy profile is shown in Fig. 6(b). As can be seen from the figure labels, the potential barrier between these two geometries is calculated to be  $14 \text{ cm}^{-1}$ . Since this is a 0 K calculation, we

must consider whether this barrier is enough to bind the cluster at real formation temperatures. The normal mode of the least stable geometry which translates the argon along this coordinate has a calculated frequency of  $16.6 \text{ cm}^{-1}$ . This corresponds to a zero point energy of  $8.3 \text{ cm}^{-1}$ . At a cluster temperature of 10 K, the cluster will have enough energy to get over this barrier into the deeper well. The cluster temperature is significantly higher than 10 K when the cluster forms and then is further cooled in the expansion. Therefore, the least stable calculated geometry should not exist in the molecular beam. The two cluster geometries which these calculations predict are labeled I and II in Fig. 6(a), with binding energies of 232 and  $200 \text{ cm}^{-1}$ , respectively. The barrier between these two conformations is greater than  $50 \text{ cm}^{-1}$  and is probably sufficient to isolate the two conformers.

For higher order clusters, the calculated geometries are simply the different combinations of  $\text{DABCO}(\text{Ar})_1$  cluster binding sites and the binding energies are additive to within 5%.

The qualitative results of this calculation and the relative energies of the different cluster geometries are quite helpful in understanding the experimental data and are in general agreement with the observations.

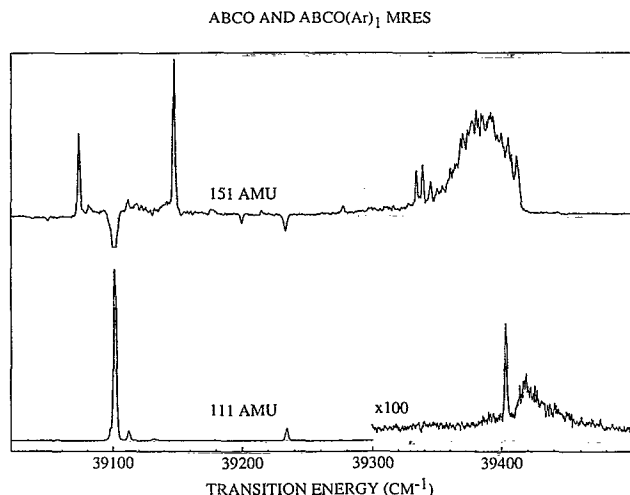


FIG. 7. One photon, two color (1+1) MRES of the ABCO(Ar)<sub>1</sub> cluster (top trace) and the ABCO bare molecule (bottom trace). The ABCO electronic origin ( $0_0^0$ ) at 39 101.1 cm<sup>-1</sup> is one photon allowed. The MRES signal in the 111 amu mass channel is multiplied by 100 above 39 300 cm<sup>-1</sup>. This illustrates that the cluster giving rise to the broad feature in the 151 amu mass channel dissociates at 39 416 cm<sup>-1</sup> and its signal simultaneously appears in the 111 amu mass channel.

## B. ABCO(Ar)<sub>1</sub>

### 1. Experiment

The bottom trace in Fig. 7 shows the one photon excitation, two color ionization, MRES of ABCO in the region if its  $3s \leftarrow n$  origin ( $0_0^0$  transition). This spectrum is in agreement with a previously reported jet-cooled MPI spectrum.<sup>5</sup> The top trace in Fig. 7 shows the one photon excitation, two color ionization MRES of the ABCO(Ar)<sub>1</sub> cluster. This spectrum has three prominent features: two intense sharp features and one intense broad feature which is characterized by a sharp decrease in intensity on its high energy side. The negative peaks are due to detector saturation from the bare ABCO molecule signal which is approximately 100 times more intense than the cluster signal. The lowest energy feature in the 151 amu mass channel is sharp and shifted 28 cm<sup>-1</sup> to the red of the bare molecule origin. The second sharp feature in this mass channel is blue shifted by 47 cm<sup>-1</sup> with respect to the bare molecule origin. The broad feature observed in this mass channel begins approximately 245 cm<sup>-1</sup> to the blue of the bare molecule origin and vanishes about 70 cm<sup>-1</sup> further to the blue. This sharp decrease in signal in the ABCO(Ar)<sub>1</sub> mass channel (151 amu) is coincident with the appearance of signal in the bare ABCO molecule mass channel (111 amu). Similar behavior is described above for the case of the DABCO(Ar)<sub>1</sub> cluster in Sec. III A 1 and shown in Fig. 3. In the bottom trace of Fig. 7 the spectral intensities at transition energies greater than 39 300 cm<sup>-1</sup> have been multiplied by 100 to demonstrate this. The broad signal which appears in the bare ABCO molecule mass channel (111 amu) is not present when argon is absent from the molecular beam and is indicative of cluster dissociation.

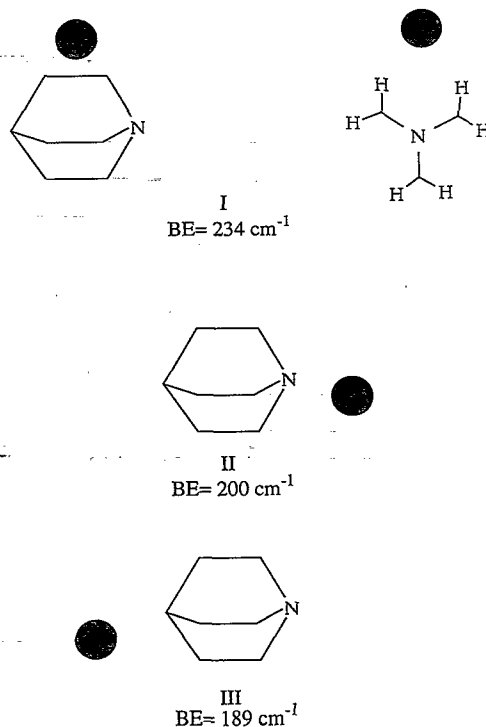


FIG. 8. Three minimum energy geometries of the ABCO(Ar)<sub>1</sub> cluster simulated with a Lennard-Jones-type potential and their binding energies.

Clusters with more than one argon atom are not observed for ABCO. This is probably due to the relatively low signal intensity of the bare ABCO molecule. The ABCO spectrum is roughly five times less intense than the DABCO spectrum.

### 2. Calculation

Cluster geometry calculations for the ABCO(Ar)<sub>1</sub> cluster produce four minimum energy configurations. Three of these configurations are analogous to those described above for the DABCO(Ar)<sub>1</sub> cluster. Since ABCO does not have a  $\sigma_h$  plane, a fourth configuration exists with the argon at the end of the molecule near the tertiary carbon and just off the  $C_3$  axis. The least stable calculated geometry will not exist in the molecular beam for reasons discussed for DABCO(Ar)<sub>1</sub> in Sec. III A 2. The three remaining configurations are shown in Fig. 8, labeled I, II, and III, with binding energies of 234, 200, and 189 cm<sup>-1</sup>, respectively. A normal mode analysis of these calculated cluster geometries produce vdW mode frequencies from 12 to 34 cm<sup>-1</sup>.

## IV. DISCUSSION

The following discussion is divided into two parts. The first part addresses the assignment of spectral features to cluster geometries. Both the sharp and broad spectral features are assigned as  $0_0^0$  transitions for different cluster geometries. The DABCO(Ar)<sub>1</sub> and ABCO(Ar)<sub>1</sub> spectra are

then compared and the conclusions from this comparison are used to assign each of these features to specific calculated cluster geometries. The spectral features arising from  $\text{DABCO}(\text{Ar})_2$  and  $\text{DABCO}(\text{Ar})_3$  cluster species are then assigned to specific calculated cluster geometries by an analogous treatment. The second part of this section presents an interpretation of these assignments in terms of the form of the intermolecular potential, the spatial distribution of the Rydberg orbital, and the amount of delocalization of the Rydberg orbital in  $\text{DABCO}(\text{Ar})_n$  clusters.

## A. Assignment of cluster geometries

### 1. General features

The lowest energy transitions in all of the cluster spectra are sharp. The sharp features in traces (a), (b), and (c) of Fig. 2 are identified from the nozzle/laser timing delay studies as being due to the  $\text{DABCO}(\text{Ar})_1$ ,  $\text{DABCO}(\text{Ar})_2$ ,  $\text{DABCO}(\text{Ar})_3$  clusters, respectively. They are assigned as cluster  $0_0^0$  transitions for four reasons. First, the  $3s \leftarrow n$  Rydberg transition of 1,4-dioxane clustered with various nonpolar solvents displays only blue shifted spectra.<sup>3</sup> Second, no cluster signal to the red of these transitions is observed. Third, no DABCO vibronic transitions (one or two photon allowed) are within  $100 \text{ cm}^{-1}$  of the origin in the bare molecule spectrum. Fourth, an additive  $100 \text{ cm}^{-1}$  blue shift per additional argon atom is observed and this additivity is common for a homologous series of clusters.<sup>13</sup> The additional features in the region of each of these sharp cluster  $0_0^0$  transitions are due to cluster hot bands or vdW modes. There is extensive sequence band structure in the bare molecule spectrum which has been previously assigned;<sup>5,4</sup> however, the population depletion study of the  $\text{DABCO}(\text{Ar})_1$  cluster provides evidence against the assignment of these major features in trace (a) of Fig. 2 as hot bands. Therefore, these features must be due to cluster vdW modes.

All other spectral features are broad and share some common characteristics. They are identified by the population depletion and nozzle/laser timing delay studies as being due to clusters with geometries which are different from those of the sharp features and from each other. Their blue shifts are larger than those of the sharp features arising from clusters with identical mass. Also, they are all shown to dissociate into the next lower mass channel. The sharp and the broad  $0_0^0$  transitions are one photon allowed for the DABCO clusters, while in the DABCO bare molecule the  $0_0^0$  transition is one photon forbidden and two photon allowed.

The top trace of Fig. 7 shows the  $\text{ABCO}(\text{Ar})_1$  spectrum. Similar to the  $\text{DABCO}(\text{Ar})_n$  spectra, this spectrum possesses both a blue shifted sharp feature, and a blue shifted broad feature; however, in addition to these, a sharp red shifted feature is also observed. This is the first observation of a red shifted  $0_0^0$  transition for a Rydberg transition in a molecular cluster.

### 2. $\text{DABCO}(\text{Ar})_1$ and $\text{ABCO}(\text{Ar})_1$

A comparison of the  $\text{DABCO}(\text{Ar})_1$  and  $\text{ABCO}(\text{Ar})_1$  spectra shows that, in both these spectra, sharp and broad

blue shifted features are found. Additionally, the broad blue shifted features in both spectra are shown to dissociate into the next lower mass channel. An additional feature is present in  $\text{ABCO}(\text{Ar})_1$  spectrum which is sharp and red-shifted. The appearance of this new feature in the  $\text{ABCO}(\text{Ar})_1$  cluster spectrum is coincident with the calculation of an additional cluster geometry, which is  $\text{ABCO}(\text{Ar})_1$  geometry III shown in Fig. 8. In this cluster geometry, the argon atom is much further from the ABCO nitrogen than is possible in the  $\text{DABCO}(\text{Ar})_1$  cluster. Previous studies have shown that nonpolar, external perturbers interact repulsively with the spatially large  $3s$  molecular Rydberg orbitals, resulting in blue shifted spectral origins.<sup>3,14</sup> The red shift of the new feature in the  $\text{ABCO}(\text{Ar})_1$  spectrum suggests that the solute-solvent distance in this cluster is large enough so that the atom-molecule interaction is attractive instead of repulsive. This favorable interaction may be due to the large polarizability<sup>15</sup> of the extravalent  $3s$  orbital. In  $\text{ABCO}(\text{Ar})_1$  geometry III, the solvent atom is located far enough from the chromophore atom to make this type of interaction possible.

The sharp, red shifted  $\text{ABCO}(\text{Ar})_1$  spectral feature is assigned to the  $\text{ABCO}(\text{Ar})_1$  geometry III because of the large separation between the argon atom and the nitrogen chromophore in this cluster geometry. Based on this relationship between binding site and chromophore atom, the  $\text{DABCO}(\text{Ar})_1$  and  $\text{ABCO}(\text{Ar})_1$  calculated geometries I and II are assigned to the sharp blue shifted feature and the broad blue shifted feature, respectively. Cluster geometry I has the argon atom nearer to the nitrogen atom than the  $\text{ABCO}(\text{Ar})_1$  geometry III. In this configuration, the argon atom is closer to the nitrogen chromophore and is expected to interact repulsively with the  $3s$  orbital upon excitation. This decreases the cluster binding energy in the excited state relative to the ground state and results in a blue shift of the cluster origin. In geometry II, the argon atom is closest to the nitrogen atom. In this binding site, the argon atom interacts strongly with the excited state nitrogen  $3s$  orbital, resulting in a large blue shift of the cluster origin and, at high vibrational energies in the excited state, results in cluster dissociation. A summary of spectral shifts and their assigned  $\text{DABCO}(\text{Ar})_n$  and  $\text{ABCO}(\text{Ar})_1$  calculated cluster geometries is found in Fig. 9. The  $\text{DABCO}(\text{Ar})_{2,3}$  cluster geometries, represented in two dimensions in this figure, are combinations of the  $\text{DABCO}(\text{Ar})_1$  geometries I and II.

The cluster geometry calculations predict ground state geometries and their binding energies. These calculations cannot model the excited state of the cluster. Since we are able to assign spectral features to specific calculated cluster geometries in the present study, then it is possible to predict the excited state binding energies from these calculations. If the cluster spectral shift is taken to be the difference between the ground and excited state binding energies, then subtraction of the spectral shift from the ground state binding energy yields the predicted excited

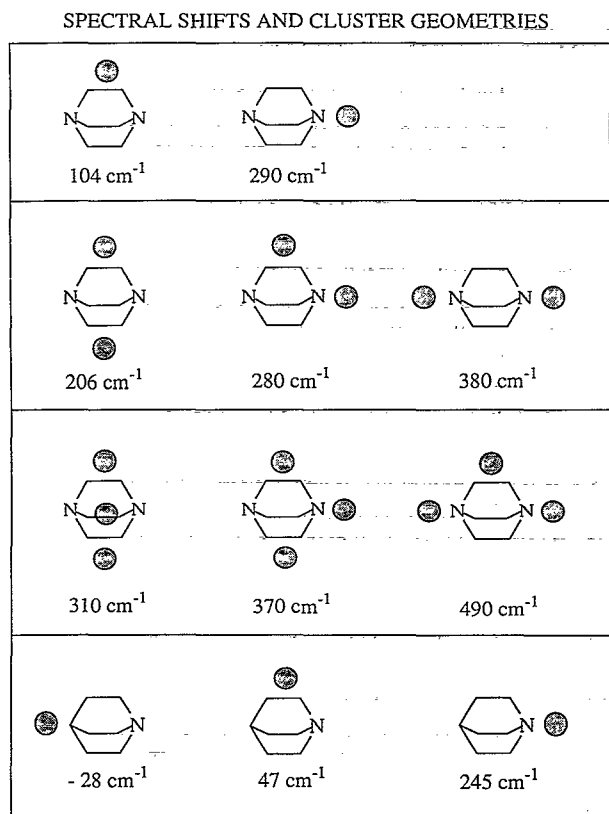


FIG. 9. Binding sites for DABCO(Ar)<sub>1,2,3</sub> and ABCO(Ar)<sub>1</sub> clusters and the shift of the assigned spectral feature. The spectral shifts are relative to the DABCO bare molecule origin ( $0_0^0$ ) at 35 786.3 cm<sup>-1</sup>. The DABCO(Ar)<sub>2,3</sub> cluster geometries, represented in two dimensions in this figure, are combinations of the DABCO(Ar)<sub>1</sub> geometries I and II.

state binding energy. This analysis is contingent upon the observation of the cluster  $0_0^0$  transition. The  $0_0^0$  transition is certainly observed in the DABCO(Ar)<sub>n</sub> and ABCO(Ar)<sub>1</sub> spectra for cluster geometries resulting in sharp spectral features; however, this is not necessarily true for clusters associated with broad spectral features (see Sec. IV B 1). The estimation of excited state binding energies for these latter cluster geometries assumes that the low energy edge of the broad features is the  $0_0^0$  transition energy. If this is not true, then this treatment will underestimate the excited state binding energy. The following discussion examines the ability of this type of analysis to predict excited state binding energies for clusters which give rise to the spectrum in the 152 amu mass channel [trace (a) of Fig. 2]. These three spectral features are representative of the three different types of features found in the DABCO(Ar)<sub>n</sub> and ABCO(Ar)<sub>1</sub> spectra.

The first sharp feature in trace (a) of Fig. 2 is assigned to DABCO(Ar)<sub>1</sub> cluster geometry I and calculations predict its ground state binding energy to be 232 cm<sup>-1</sup>. Subtraction of the 104 cm<sup>-1</sup> blue shift from this result yields an excited state binding energy of 128 cm<sup>-1</sup>. This predicts that this cluster is bound in the excited state and is in agreement with the experimental observation that it does not dissociate. The second feature in trace (a) of Fig. 2 is

assigned to DABCO(Ar)<sub>1</sub> cluster geometry II and calculations predict its ground state binding energy to be 200 cm<sup>-1</sup>. Subtraction of the 290 cm<sup>-1</sup> blue shift predicts that this cluster will be unbound by 90 cm<sup>-1</sup> in the excited state. However, Fig. 3 demonstrates that this cluster is bound for at least 20 cm<sup>-1</sup> in the excited state before it dissociates sharply. This sharp dissociation shows that the calculated ground state binding energy is at least 110 cm<sup>-1</sup> too small. The third feature in trace (a) of Fig. 2 has a spectral shift of 380 cm<sup>-1</sup> and is assigned to a DABCO(Ar)<sub>2</sub> cluster geometry which is shown in Fig. 9. Cluster geometry calculations predict the ground state binding energy for this cluster to be 402 cm<sup>-1</sup>. Subtraction of the blue shift from the ground state binding energy yields an excited state binding energy of approximately 22 cm<sup>-1</sup> for this cluster. This cluster is observed experimentally to dissociate which suggests that the calculated ground state binding energy for this cluster is at least about 20 cm<sup>-1</sup> too large.

The possibility that a cluster will rearrange to a more stable geometry rather than dissociate can be eliminated because the cluster always maintains the energy of excitation under these isolated conditions. Additionally, for small clusters dissociation occurs within picoseconds following intracuster vibrational energy redistribution from the DABCO modes to the van der Waals modes.<sup>16</sup>

### 3. DABCO(Ar)<sub>2</sub>

Three DABCO(Ar)<sub>2</sub> spectral features which appear in the 192 and 152 amu mass channels can be identified. These features are assigned as spectral origins for three different calculated cluster geometries. This assignment is based on an analysis analogous to that for the DABCO(Ar)<sub>1</sub> and ABCO(Ar)<sub>1</sub> cluster spectra and geometry calculations. Transition energies for the sharp features and the approximate onset of intensity for the broad features are listed in Table I. The broad feature in the 192 amu mass channel, with a 280 cm<sup>-1</sup> blue shift, shows that the cluster begins to dissociate at about 320 cm<sup>-1</sup> and the product from that dissociation can be seen in the 152 amu mass channel. The third DABCO(Ar)<sub>2</sub> feature is seen in the 152 amu mass channel with a blue shift of 380 cm<sup>-1</sup> and with intensity similar to that for the DABCO(Ar)<sub>1</sub> cluster. This strong intensity in the dissociation mass channel suggests that this cluster is completely dissociating.

These DABCO(Ar)<sub>2</sub> spectral features can also be assigned to specific calculated cluster geometries. These assignments are shown in Fig. 9. The sharp features are assigned to the cluster geometry with both argon atoms in the  $\sigma_h$  plane. Notice that these features have twice the blue shift of DABCO(Ar)<sub>1</sub> geometry I. The first broad feature, at 280 cm<sup>-1</sup>, is assigned to a calculated cluster geometry with one argon atom in the  $\sigma_h$  plane (site I) and one near a DABCO nitrogen atom along the  $C_3$  axis (site II). The third feature has the largest blue shift, at 380 cm<sup>-1</sup> in the 152 amu mass channel, and is assigned to the calculated cluster geometry with the two argon atoms near different DABCO nitrogen atoms along the  $C_3$  axis. In this

cluster geometry, the interaction between solvent argon atoms and  $3s$  nitrogens is greatest.

#### 4. DABCO(Ar)<sub>3</sub>

Three DABCO(Ar)<sub>3</sub> spectral features appear in the 232 and 192 amu mass channels. The broad feature shifted 380 cm<sup>-1</sup> in the 192 amu mass channel is shown above to be due to a DABCO(Ar)<sub>3</sub> cluster. The DABCO(Ar)<sub>3</sub> cluster giving rise to this feature must completely dissociate since this signal does not appear at all in the 232 amu mass channel. The third DABCO(Ar)<sub>3</sub> feature is also seen through dissociation in the 192 amu mass channel, shifted 490 cm<sup>-1</sup>.

These DABCO(Ar)<sub>3</sub> spectral features are assigned to specific calculated cluster geometries based on the extent the solvent atoms are expected to interact with the DABCO nitrogen  $3s$  orbital. These assignments are shown in Fig. 9. The sharp features are assigned to the cluster geometry with all three of the argon atoms in the  $\sigma_h$  plane. The blue shift of this feature is approximately three times that of the sharp features assigned to DABCO(Ar)<sub>1</sub> geometry I. The first broad feature, shifted 370 cm<sup>-1</sup> in the 192 amu mass channel, is assigned to a calculated cluster geometry with two argon atoms in the  $\sigma_h$  plane and the third argon atom is near a DABCO nitrogen atom along the C<sub>3</sub> axis. In this configuration, the argon interaction with the DABCO  $3s$  nitrogens will be intermediate to that of the other two possible geometries. This is consistent with its blue shift which is intermediate to the other two DABCO(Ar)<sub>3</sub> spectral features. Finally, the second broad feature, shifted 490 cm<sup>-1</sup> in the 192 amu mass channel, is assigned to the third possible calculated cluster geometry in which one argon atom is in the  $\sigma_h$  plane and the other two argon atoms are near different DABCO nitrogen atoms along the C<sub>3</sub> axis. In this geometry, the solvent interaction with the Rydberg orbital should be greatest.

#### B. Implications for molecular Rydberg state properties

The above discussion of the effects of clustering on the  $2p3s \leftarrow 2p^2$  Rydberg transition in DABCO and ABCO provides information about three fundamental properties of molecular Rydberg states. These properties include the effect of Rydberg excitation upon the intermolecular interaction, the effect of solvent binding site on this interaction, and amount of localized, atomic-like character or delocalized character of the molecular Rydberg orbital. These three questions are addressed sequentially below.

##### 1. Intermolecular potential

The three different types of features observed in the  $3s \leftarrow n$  spectra of the DABCO(Ar)<sub>n</sub> and ABCO(Ar)<sub>1</sub> clusters can be related to the cluster intermolecular interaction. The effect of the Rydberg transition on this interaction dictates the characteristics of the spectral feature. The DABCO(Ar)<sub>n</sub> cluster spectra may be used to illustrate this: sharp features in these spectra show no signs of dissociation; broad features are partially detected in the DABCO(Ar)<sub>n</sub> mass channel until the signal sharp-

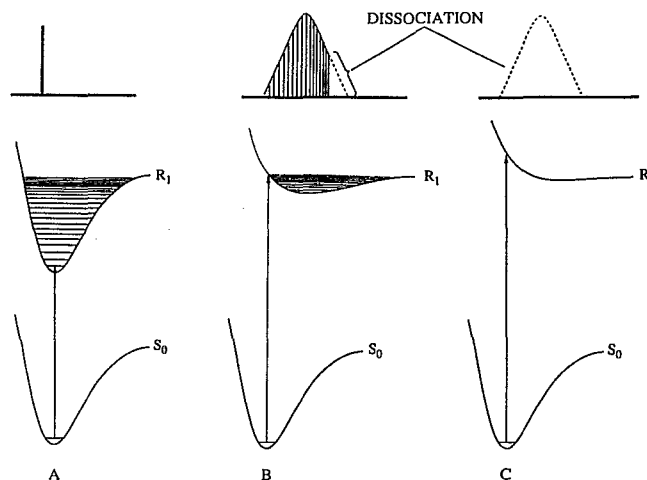


FIG. 10. Three proposed excited state potentials which model the three different types of spectral features. Above each is a stick diagram which illustrates what type spectrum is expected to result from it. The dashed lines in C indicate that the signal will not be present in the parent cluster mass channel due to dissociation.

ly disappears and is coincidentally detected in the DABCO(Ar)<sub>n-1</sub> mass channel; and broad features which are not detected at all in the DABCO(Ar)<sub>n</sub> mass channel, but are detected in the DABCO(Ar)<sub>n-1</sub> mass channel. The first and second conditions are also seen in the ABCO(Ar)<sub>1</sub> spectrum. Pictorial representations of the excited state potentials which explain these spectral characteristics are shown in Fig. 10 along with the associated line spectra. These excited state potentials represent the totally symmetric atom-molecule stretching mode, which we believe is most likely the dissociation coordinate. The excited state potential A is only slightly displaced along the intermolecular coordinate and with a smaller binding energy than the ground state (for a blue shifted  $0_0^0$  transition). The excitation is  $v' = 0 \leftarrow v'' = 0$  and the resulting spectral feature is a sharp line at the  $0_0^0$  transition energy. Potential B has a more significant displacement along the intermolecular coordinate and the excited state is only slightly bound, with a binding energy which is much less than that of the ground state. In this case, the bound vibrational levels are very closely spaced, and due to the shift of the excited state potential the transition will have some Franck-Condon overlap with a number of excited state vibrational levels which are bound and also some which are not bound. The resulting spectrum includes transitions to the bound states which result in a group of congested lines in the cluster mass channel, and transitions to the unbound states which result in the dissociation of the cluster and a broad feature in the next lower mass channel. Potential C is repulsive along the intermolecular coordinate and has a very large displacement. In this case, all excitations are to states which are not bound and thereby cause the cluster to dissociate. This results in a broad feature in the next lower mass channel. Excited state potential C has been proposed

by Robin *et al.* to explain the effects of pressure on gas phase vacuum ultraviolet spectra of Rydberg transitions.<sup>1,14</sup>

## 2. The effect of solvent binding site

The excited state van der Waals potentials can be related to the different solvent binding sites in terms of the type of interaction they produce between the solvent and the Rydberg orbital. This relationship provides information about the spatial distribution of the molecular Rydberg orbital. Argon has only two possible binding sites when clustered with DABCO, in the  $\sigma_h$  plane or along the  $C_3$  axis. The major difference between these two sites is the distance of the solvent atom from the nitrogen 3s center. The interaction between the argon and the excited Rydberg electron is expected to be much greater when the argon binds along the  $C_3$  axis near the nitrogen. This binding site [ABCO(Ar)<sub>1</sub> or DABCO(Ar)<sub>1</sub>] results in excited state potentials B and C in which the excitation is either partially or totally dissociative. Alternatively, clusters in which the argon binds in the  $\sigma_h$  plane [ABCO(Ar)<sub>1</sub> or DABCO(Ar)<sub>1</sub>] result in an excited state potential of type A in which the cluster is only somewhat destabilized upon excitation ( $\sim 100 \text{ cm}^{-1}$ ). For the ABCO(Ar)<sub>1</sub> cluster a third possibility exists in which the argon atom binds along the  $C_3$  axis, opposite the nitrogen and near the tertiary carbon. The argon atom is furthest from the Rydberg orbital in this case. Evidently, this distance is large enough to make the interaction between the argon atom, the valence electrons, and the nitrogen 3s orbital stabilize the cluster through dispersion forces. This results in an excited state potential which is similar to A in Fig. 10, except it is displaced to smaller intermolecular distance, and the excited state binding energy is greater than that of the ground state.

## 3. Delocalization of DABCO nitrogen 3s orbital

The ABCO(Ar)<sub>1</sub> cluster results can provide insight into the amount of localization or delocalization of the 3s Rydberg orbital in the DABCO(Ar)<sub>1</sub> cluster. The presence of a single nitrogen chromophore atom in ABCO makes this possible. The red shifted feature in the ABCO(Ar)<sub>1</sub> spectrum suggests that the Rydberg orbital is localized near the nitrogen atom. If the 3s orbital in ABCO were completely delocalized, then it might be expected that no solvent binding site will place the argon atom far enough away from the large radial distribution of the Rydberg electron to avoid a repulsive interaction.

If the excitation is localized on a single nitrogen atom in the DABCO(Ar)<sub>1</sub> cluster, then like the ABCO(Ar)<sub>1</sub> cluster, three inequivalent binding sites would be observed. The third binding site would exist for the argon bound near the nitrogen atom whose lone pair electron is not excited. This is not observed in the DABCO(Ar)<sub>n</sub> spectra. If the molecular Rydberg orbital is a combination of the two nitrogen atom 3s orbitals, then it will be delocalized. For excitation to a delocalized orbital of this type, the binding sites next to the two nitrogens would be equivalent and only two inequivalent cluster geometries would exist. This

situation is observed in the DABCO(Ar)<sub>n</sub> spectra. The conclusion is that the DABCO 3s Rydberg orbital is delocalized between the two nitrogen atoms and exists over the entire molecular framework.

## V. SUMMARY AND CONCLUSION

Two color 1+1 mass resolved excitation spectroscopy (MRES) is used to obtain molecular Rydberg spectra of azabicyclo[2.2.2]octane (ABCO) and diazabicyclo[2.2.2]octane (DABCO) clustered with argon. Nozzle/laser timing delay studies are employed together with time-of-flight mass spectroscopy to identify cluster composition. Population depletion techniques are used to differentiate between clusters with the same mass, but different geometries. All of these results, combined with cluster geometry calculations, are used to assign spectral features to specific cluster geometries. The DABCO(Ar)<sub>1</sub> cluster has two different geometries. One geometry has an argon binding site in the DABCO  $\sigma_h$  plane, gives rise to a sharp blue shifted spectral origin, and does not dissociate upon excitation. The other geometry has an argon binding site near the nitrogen atom along the  $C_3$  axis, gives rise to a broad blue shifted spectral feature, and partially dissociates into the lower mass channel upon excitation.

The DABCO(Ar)<sub>2</sub> and DABCO(Ar)<sub>3</sub> clusters are both determined to have three distinct geometries. Three sets of geometries for these clusters may be described. Geometries in which all of the argon atoms are in the  $\sigma_h$  plane result in sharp, blue shifted spectral features. The blue shifts for these geometries are additive for the DABCO(Ar)<sub>1,2,3</sub> clusters. Geometries in which only one argon atom is near the nitrogen atom along the  $C_3$  axis result in broad, blue shifted spectral features and their Rydberg transitions are either partially or completely dissociative. Geometries in which two argon atoms are along the  $C_3$  axis near different nitrogen atoms give rise to broad, blue shifted spectral features and their transitions are completely dissociative.

Three ABCO(Ar)<sub>1</sub> cluster geometries can be identified. Two of these geometries are analogous to DABCO(Ar)<sub>1</sub> geometries I and II. These two ABCO(Ar)<sub>1</sub> geometries generate spectral features similar to their DABCO(Ar)<sub>1</sub> analogs. The third geometry has an argon binding site which is opposite the nitrogen atom and next to the tertiary carbon, along the  $C_3$  axis. This geometry generates a sharp, red shifted spectral feature which is not seen in the DABCO(Ar)<sub>1</sub> cluster spectra. This is the first red shifted origin observed in the molecular Rydberg spectrum of a cluster. The red shift is attributed to an interaction between the argon atom and the 3s Rydberg orbital which stabilizes the excited state cluster. This type of interaction is made possible by the large separation between the solvent and chromophore atoms.

These data result in the important conclusion that the nature of the intermolecular potential for an excited Rydberg state cluster is dependent on the proximity of the solvent binding site to the chromophore atom. The red shifted feature in the ABCO(Ar)<sub>1</sub> cluster spectrum indicates that its molecular Rydberg orbital is mostly localized.

The lack of a similar feature in the DABCO(Ar)<sub>1</sub> cluster spectrum suggests that its molecular Rydberg orbital is delocalized.

#### ACKNOWLEDGMENT

Work supported in part by a grant from ARO-D.

<sup>1</sup>(a) M. B. Robin, *Higher Excited States of Polyatomic Molecules* (Academic, New York, 1974), Vol. I; (b) *Higher Excited States of Polyatomic Molecules* (Academic, New York, 1975), Vol. II.

<sup>2</sup>S. H. Lin, Y. Fujimura, H. J. Neusser, and E. W. Schlag, *Multiphoton Spectroscopy of Molecules* (Academic, New York, 1984).

<sup>3</sup>P. O. Moreno, Q. Y. Shang, and E. R. Bernstein, *J. Chem. Phys.* **97**, 2869 (1992).

<sup>4</sup>D. H. Parker and P. Avouris, *J. Chem. Phys.* **71**, 1241 (1979).

<sup>5</sup>N. Gonohe, N. Yatsuda, N. Mikami, and M. Ito, *Bull. Chem. Soc. Jpn.* **55**, 2796 (1982).

<sup>6</sup>R. Hoffman, *Acc. Chem. Res.* **4**, 1 (1971).

<sup>7</sup>K. Ohno, T. Ishida, Y. Naitoh, and Y. Izumi, *J. Am. Chem. Soc.* **107**, 8082 (1985).

<sup>8</sup>E. R. Bernstein, K. Law, and M. Schauer, *J. Chem. Phys.* **80**, 207 (1984).

<sup>9</sup>Q. Y. Shang and E. R. Bernstein, *J. Chem. Phys.* **97**, 60 (1992).

<sup>10</sup>S. Li and E. R. Bernstein, *J. Chem. Phys.* **97**, 7383 (1992).

<sup>11</sup>(a) G. Nemethy, M. S. Pottle, and H. A. Scheraga, *J. Phys. Chem.* **87**, 1883 (1983); (b) J. F. Yan, F. A. Momany, R. Hoffmann, and H. A. Scheraga, *ibid.* **74**, 420 (1970); (c) F. A. Momany, R. F. McGuire, J. F. Yan, and H. A. Scheraga, *ibid.* **74**, 2424 (1970); (d) R. F. McGuire, F. A. Momany, and H. A. Scheraga, *ibid.* **76**, 375 (1972).

<sup>12</sup>S. Li and E. R. Bernstein, *J. Chem. Phys.* **95**, 1577 (1991).

<sup>13</sup>*Atomic and Molecular Clusters*, edited by E. R. Bernstein (Elsevier, New York, 1990).

<sup>14</sup>M. B. Robin and N. A. Kuebler, *J. Mol. Spectrosc.* **33**, 274 (1970).

<sup>15</sup>G. C. Causley and B. R. Russel, *J. Am. Chem. Soc.* **101**, 5573 (1979).

<sup>16</sup>(a) M. R. Nimlos, M. A. Young, E. R. Bernstein, and D. F. Kelley, *J. Chem. Phys.* **91**, 5268 (1989); (b) M. F. Hineman, S. K. Kim, E. R. Bernstein, and D. F. Kelley, *J. Chem. Phys.* **96**, 4904 (1992).